Journal of Colloid and Interface Science 603 (2021) 182–190

Contents lists available at ScienceDirect

Journal of Colloid and Interface Science

journal homepage: www.elsevier.com/locate/jcis

Regular Article

Nicotinamide-based supergelator self-assembling via asymmetric hydrogen bonding NH···OC and H···Br⁻ pattern for reusable, moldable and self-healable nontoxic fuel gels

Peter Kasak [a,*], Peter Hrobárik [b,c,*], Josef Osička [d], Dominika Soláriková [e], Branislav Horváth [f], Jan Tkac [g], Kishor K. Sadasivuni [a], Mariam A. AlMaadeed [a], Roman Mikláš [e,*]

[a] Center for Advanced Materials, Qatar University, POBox 2713, Doha, Qatar
[b] Laboratory for Advanced Materials (LAM), Comenius University Science Park, Ilkovičova 8, SK-84215 Bratislava, Slovakia
[c] Department of Inorganic Chemistry, Faculty of Natural Sciences, Comenius University, Ilkovičova 6, SK-84215 Bratislava, Slovakia
[d] Centre of Polymer Systems, University Institute, Tomas Bata University in Zlin, Trida T. Bati 5678, CZ-76001 Zlin, Czech Republic
[e] Department of Chemical Theory of Drugs, Faculty of Pharmacy, Comenius University, Kalinčiakova 8, SK-83104 Bratislava, Slovakia
[f] Laboratory of Nuclear Magnetic Resonance, Faculty of Pharmacy, Comenius University in Bratislava, Odbojárov 10, SK-83232 Bratislava, Slovakia
[g] Institute of Chemistry, Slovak Academy of Sciences, Dúbravska cesta 9, SK-84538 Bratislava, Slovakia

GRAPHICAL ABSTRACT

ARTICLE INFO

Article history:
Received 28 March 2021
Revised 10 June 2021
Accepted 11 June 2021
Available online 15 June 2021

Keywords:
Fuel gel
Supergelation
Nicotinamide derivative
Low-molecular weight gelators
DFT calculations
Circular dichroism

ABSTRACT

Hypothesis: Development of highly efficient low-molecular weight gelators (LMWGs) for safe energy storage materials is of great demand. Energy storage materials as fuel gels are often achieved by construction of hybrid organic frameworks capable of multiple noncovalent interactions in self-assembly, which allow tuning required properties at the molecular level by altering individual building blocks of the LMWG. However, LMWGs have limited rechargeable capability due to their chemical instability.
Experiments: We designed, synthesized and characterized a novel, bio-inspired chiral gemini amphiphile derivative **1** containing *N*-hexadecyl aliphatic tails from quaternized nicotinamide-based segment and bromide anion showing supergelation ability in water, alcohols, aprotic polar and aromatic solvents, with critical gel concentrations as low as 0.1 and 0.035 wt% in isopropanol and water, respectively.
Findings: Nanostructural architecture of the network depended on the solvent used and showed variations in size and shape of 1D nanofibers. Supergelation is attributed to a unique asymmetric NH···OC, H···Br⁻ hydrogen bonding pattern between H-2 hydrogens from nicotinamide-based segment, amide functional groups from chiral *trans*-cyclohexane-1,2-diamide-based segment and bromide ions,

* Corresponding authors at: Center for Advanced Materials, Qatar University, POBox 2713, Doha, Qatar (P. Kasak); Laboratory for Advanced Materials (LAM), Comenius University Science Park, Ilkovičova 8, SK-84215 Bratislava, Slovakia (P. Hrobárik); Department of Chemical Theory of Drugs, Faculty of Pharmacy, Comenius University, Kalinčiakova 8, SK-83104 Bratislava, Slovakia (R. Mikláš).
E-mail addresses: peter.kasak@qu.edu.qa (P. Kasak), peter.hrobarik@uniba.sk (P. Hrobárik), miklas@fpharm.uniba.sk (R. Mikláš).

https://doi.org/10.1016/j.jcis.2021.06.071

supporting the intermolecular amide–amide interactions appearing across one strand of the self-assembly. Gels formed from **1** exhibit high stiffness, self-healing, moldable and colorable properties. In addition, isopropanol gels of **1** are attractive as reusable, shape-persistent non-toxic fuels maintaining the chemical structure with gelation efficiency for at least five consecutive burning cycles.

1. Introduction

In everyday life, gels are widely utilized in the cosmetic, food and bioengineering industries. Progressive and productive gel applications have appeared in the fields of catalysis [1], medicine [2–3], sensors [4] and nanoelectronics [5] as well as other advanced applications [6–9]. Apart from these applications, gels can be used as energy storage materials [6] or as fuel gels. The latter are commonly used for chafing dishes, emergency heating or aesthetic and decorative purposes [8]. Such materials consist of alcohol-based gelators, often limited to single-use only [10–11]. Recently, Bera and Haldar [12] developed rechargeable fuel gel based on a multicomponent mixture comprising dimethyl dipicolinate, water, KOH and MeOH. Such gel, however, suffers from the toxicity of methanol, the caustic property of hydroxide and its stability in multiple usage is limited due to hydrolysis of the gelator after several burning cycles. A similar issue with hydrolysis of gelling agent was also observed with carbohydrate-based fuel gels [13].

Gels are frequently divided based on 3D network structure formation into 1) chemical gels that comprise covalently cross-linked polymer matrices such as polyacrylamide [14] and poly (2 hydroxyethyl methacrylate) (polyHEMA) gels [15] and 2) physical gels that possess crosslinking based on physical interaction, such as polysaccharides (alginate, gellan, agar) [16–17] and proteins (gelatin) [18]-based gels. Apart of biopolymer-based physical gels, one of the most investigated are gels from low-molecular-weight gelators (LMWGs). LMWGs as molecules form gel via non-covalent interactions (such as hydrogen bonding, electrostatic forces, π–π stacking, van der Waals and hydrophobic interactions) that play a pivotal role in the unidirectional assembly of LMWGs [19,9]. Self-assembled fibrous nanostructures of LMWGs are further organized in liquid by non-covalent forces into entangled 3D networks. Bioinspired LMWGs capable of gelating both polar and nonpolar solvents include such biologically active units as cholesterol [20–22], amino acids [23–28], surfactants [29–32] and carbohydrates [33–36]. The major source of non-covalent interactions is hydrogen bonding - the most important organizing element that also stabilizes natural systems such as DNA, peptides and enzymes – and van der Waals forces, usually associated with the presence of urea/amide functional groups and long aliphatic hydrocarbon chains, respectively [37–41]. In recent years, the interaction between the anion and electron-poor aromatic ring has also been recognized as a non-covalent bonding force, called anion–π interaction [42–44], thus playing an important role in gelation phenomena as well [45].

Apart from the abovementioned biologically active fragments, nicotinamide-based gelators are rather rare [46]. It is noteworthy that nicotinamide (in literature often denoted also as niacinamide) is a part of a variety of biological systems, including vitamin B3 and the cofactor nicotinamide adenine dinucleotide (NADH/NAD^+) and its phosphate ($NADP^+$) [47–49] — all being crucial to life and playing a role in various enzymatic oxidation-reduction reactions. In addition, this fragment undergoes facile *N*-alkylation reactions, thus allowing formation of quaternary ionic compounds with feasible anion–π interactions along with van der Waals attractions between long alkyl chains. In this regard, we were curious about gelation properties and fuel gel application of a new chiral gemini amphiphilic nicotineamide-based derivative **1** (Fig. 1), the self-assembly structure of which was anticipated to display an additional anion - electron-deficient heteroarene (HetAr) interaction on top of traditional noncovalent bonding in neutral gemini gelators.

2. Experimental

2.1. Materials

Acetonitrile (HPLC grade, 99.9%), 1 bromohexadecane (Sigma Aldrich, 97%), diethylether (CentralChem, p.a. grade, 99.0%), hexane (CentralChem, p.a. grade, 99%), *trans*-cyclohexane-1,2-diamine (Acros Organics, 98%), isonicotinamide hydrochloride (Acros Organics, 97%), toluene (CentralChem, p.a. grade, 99%), benzene (CentralChem, p.a. grade, 99.8%), dimethylformamide (Sigma Aldrich, HPLC grade, 99.9%), ethanol (CentralChem, p.a. grade, 99.9%), dichloromethane (DCM, CentralChem, p.a. grade, 99.8%), isopropanol (≥99.5%, Sigma-Aldrich), KPF_6 (Sigma-Aldrich, ≥99%). Commercially available chemicals were used without further purification, if not mentioned otherwise. Pyridine (CentralChem, p.a. grade, 99.5%) was distilled prior to use from CaH_2 (Sigma-Aldrich, 95%). Methanol (CentralChem, p.a. grade, 99.5%) was dried by distillation from magnesium. Acetone (CentralChem, p.a. grade, 99.5%) was dried by distillation from sodium carbonate. Non-ionic *N*,*N*'-[(1*R*,2*R*)-cyclohexane-1,2-diyl]dinicotinamide (**4**) was prepared by reaction of enantiomerically pure (1*R*,2*R*)-cyclohexane-1,2-diamine (Sigma-Aldrich, 98%) with nicotinoyl chloride hydrochloride (Alfa-Aesar, 98%) in pyridine (Scheme S1, ESI) by the procedure described previously [50].

2.2. Synthesis of gelator 1:

1 g (3.08 mmol) of *N*,*N*'-[(1*R*,2*R*)-cyclohexane-1,2-diyl]dinicotin-amide (**4**) [50] was mixed in autoclave with 2.35 g of 1 bromohexadecane (7.7 mmol, 2.5 eq) and 15 ml of acetonitrile. Reaction mixture was heated at 150 °C for 48 h and then allowed to cool to room temperature. The resulting solid material was suspended in a mixture of diethylether : hexane (1:1, v/v, 100 ml) and filtered off to give light brown powder. The white crystalline gelators were obtained after three crystallizations from anhydrous acetone/methanol mixture. Racemic derivative *rac*-**1** was synthetized using the same method from racemic *trans*-cyclohexane-1,2-diamine.

Gelator **1**: White crystals, yield = 69%. M.p. = 175–176 °C.

^{1}H NMR ($CDCl_3$) δ 9.84 (s, 2H), 9.27 (d, J = 5.9 Hz, 2H), 9.04 (d, J = 8.1 Hz, 2H), 8.96 (d, J = 5.9 Hz, 2H), 8.14 (dd, J = 7.6 Hz, 7.6 Hz, 2H), 4.91 (t, J = 7.26 Hz, 4H, N^+–CH_2), 4.11 (s, 2H), 1.81–2.18 (m, 10*H*), 1.25–1.35 (m, 54H), 0.87 (t, J = 7.0 Hz, 6H, 2 × CH_3).

^{13}C NMR ($CDCl_3$) δ 161.0, 146.0, 144.4, 144.3, 134.3, 128.3, 62.6, 54.5, 31.9, 31.7, 31.2, 29.7 (2C), 29.6 (2C), 29.5, 29.4, 29.3, 29.1, 26.2, 24.7, 22.7, 14.1.

HRMS: Calculated for $C_{50}H_{86}N_4O_2^{2+}$, m/z = 387.3350, found 387.3383.

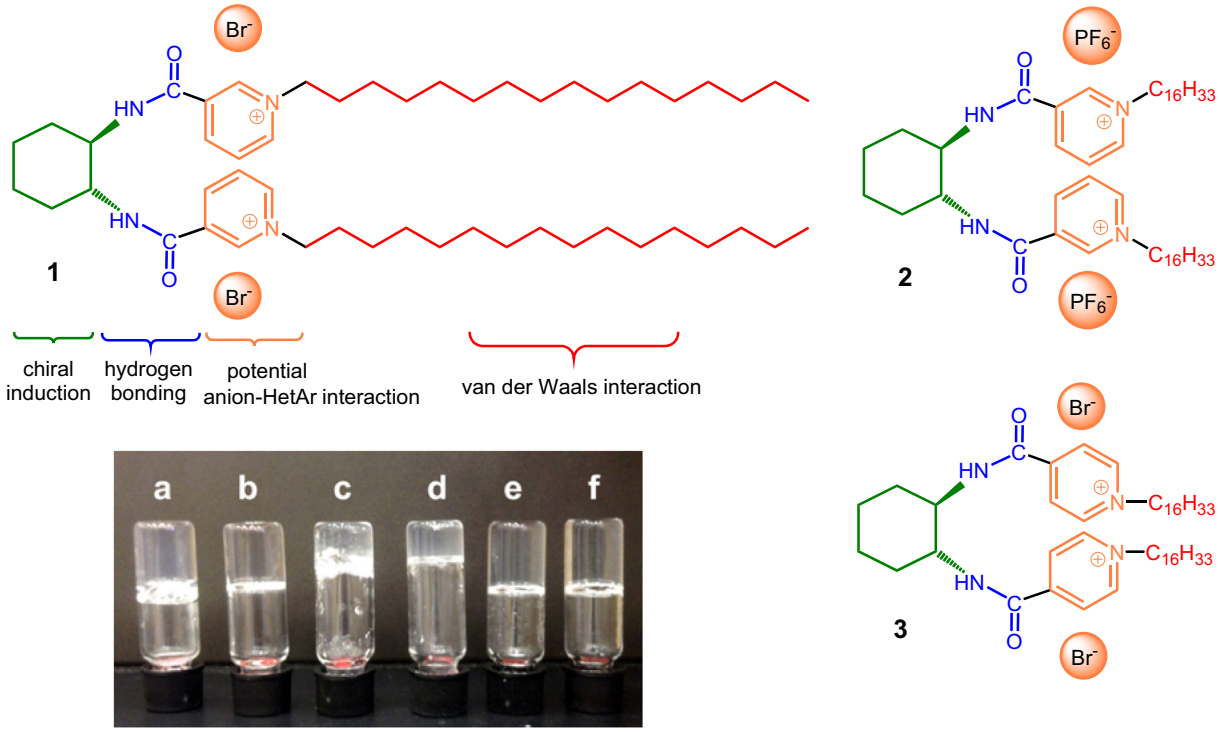

Fig. 1. Molecular structures of *N*-alkyl quaternized nicotinamide gelator (**1**), its congener with PF_6^- anion (**2**) and regioisomer containing isonicotinamide-based segment with bromide anion (**3**). Image of gels from 0.5% w/v of 1 in a) water, b) isopropanol, c) toluene, d) benzene, e) octanol and f) glycerol.

2.3. Gelation ability test

In each study, certain amount of **1** with 1 – 2 ml of solvent was added, sealed and heated. Subsequently, the sample was cooled to RT and then sample was inverted for 1 h and samples were classified as a transparent gel (G), an opaque gel (OG), a clear solution (S) or a precipitate (P). Critical gelation concentration (cgc) is defined as a concentration of the gelator, at which the gel is stable to inversion over 1 h in test tube. T_{gel} was determined by dropping-ball method and each experiment was performed in duplicate. The small ball (250 mg) was placed on the top of the gels in vials placed in oil bath, which was slowly heated (1 °C per minute). The temperature at which a ball reached a bottom of vials was recognized as a T_{gel}.

2.4. Fuel gel testing

In order to prove reusability of gelator, a burning experiment was done. An amount 2 ml of 0.5 wt% isopropanol gel was prepared in small glass container and then ignited. After all isopropanol was burnt, another 2 ml of isopropanol was added into the container and gelled again. This was repeated five times. Burning time was measured by stopwatch. Gelation ability was checked by rheology strain sweep test after each burning cycle. This examination was done in triplicate for each.

2.5. Characterizations and spectroscopic details

^1H, $^{13}C\{^1H\}$, ^{19}F and ^{31}P NMR, 2D NMR and VT experiments were recorded on a Varian Mercury 300 MHz spectrometer equipped with a 5 mm ASW 4 NUC ($^1H/^{19}F/^{13}C/^{31}P$) probe, or Varian MR400 spectrometer equipped with a 5 mm AutoX ID PFG ^1H $\{^{15}N$-$^{31}P\}$probe or 5 mm AutoX DB PFG (^1H-$^{19}F/^{15}N$-^{31}P)probe. The chemical shifts of ^1H and ^{13}C were referenced by using the TMS standard peak (in $CDCl_3$) or residual solvent peaks (D_2O/H_2O). Unified chemical shifts scale was used for ^{31}P and ^{19}F. High resolution mass specrometry (HRMS) measurements were performed on Thermo Scientific Orbitrap LTQ XL with resolution 100,000 and range 50 – 1000 *m*/*z*. CD and UV–vis spectra were performed on Jasco-815 spectrometer in various solvents as stated in the figure captions. UV/VIS spectroscopy was used to investigate gelation process using *SEC* 2000-UV/VIS Spectrometer- ALS (ALS, Japan). The Fourier transform infrared (FTIR) spectra of xerogels were collected using a attenuated total reflection ATR FT-IR Spectrometer Frontier (Perkin Elmer, Waltham, MA, USA). Rheology examination was performed to investigate viscoelastic properties of the formed gels. The rheological characteristics of composites were measured utilizing Anton Paar Rheometer Model MCR 302 (Anton Paar, Austria) connected to cone-and-plate plate geometry (CP25). Firstly, the linear viscoelastic region was investigated. Then to avoid the sample slippage, the constant shear strain 0.5% was applied. Then the frequency sweep in the range from 10^{-1} to 10^1 Hz was done. In order to study self-healing properties of prepared gels, the thixotropy sweep was measured using low strain (0.5% for 600 s) followed by high strain (100% for 50 s) repeatedly**.** The structure of xerogel fibers was observed by Scanning electron microscope Nova Nano SEM 450 (FEI, Oregon, USA) and confirmed by transmission electron microscope TECNAI G2 TEM TF20 (FEI, Oregon, USA). The samples for SEM analysis were prepared by freeze-drying to xerogels. Melting points were determined on Kofler hot bench and are uncorrected.

3. Results and discussion

In this study, nicotinamide was chosen as the electron-deficient heteroaromatic moiety due to its ubiquity in nature, non-toxic character, ready availability as well as the possibility to form ionic compounds via quaternization reactions. This segment was linked to the chiral unit of (1*R*,2*R*)-cyclohexane-1,2-diamine, while quaternization to corresponding *N*-hexadecyl pyridinium bromide

segments with long aliphatic tails was utilized as a promotor of van der Waals interactions commonly used in LMWGs.

Overall, the synthesis of **1** consists of two simple steps. Enantiomerically pure (1*R*,2*R*)- cyclohexane-1,2-diamine reacted with nicotinoyl chloride hydrochloride in the presence of pyridine as a base and subsequently quaternization of both pyridine moieties was carried out with hexadecylbromide under high pressure conditions to obtain good yields of **1**. Control compounds *rac*-**1**, hexafluorophosphate salt **2** (congener of **1** with PF_6^- anion instead of Br^-) and bromide **3** containing regioisomeric isonicotinamide-based segment instead of nicotinamide one were also synthesized (see Fig. 1 for structures and ESI† for details) in order to get a better understanding of the relationship between the molecular structure and the gelation properties. Ability to form gels was studied for a range of solvents, and the results are summarized in Table S1, ESI.

Generally, precipitation or impossibility to dissolve **1** was observed in highly non-polar aliphatic solvents, such as hexane, hexadecane and aprotic solvents, such as acetone, acetonitrile, ethyl acetate and diethyl ether. Apart from these cases, **1** was found to serve as a supergelator, the critical gelator concentration (cgc) of which was high below 1 wt% for very non-polar aromatic solvents such as benzene (0.2%) or toluene (0.1%), for polar aprotic solvents such as DMF (0.5%) as well as for polar protic solvents such as isopropanol (0.1%) and glycerol (0.05%). In water, cgc reached 0.035 wt% (Fig S18, ESI), corresponding to the concentration 0.371 mM (or 0.35 $mg.ml^{-1}$), at which one molecule of **1** immobilizes by visible rigidification almost 150,000 water molecules, which is close to the highest value obtained among low-molecular-weight hydrogelators. It is noteworthy that in rheological study, gel-like behavior with higher G‘ over G“ was observed up to 0.02 wt%; however, this gel was not considered with the lowest cgc since it was not stable for 1 h as described in section about gelation ability (see Fig. S19 and ESI† for details). **1** clearly also outperforms structurally related LMWGs derived from cyclohexane-1,2-diamine or cyclohexane-1,2-dicarboxylic acid (with cgc of 3–50 $mg.ml^{-1}$) in various non-polar and polar solvents [51–52].

Racemic derivative *rac*-**1** showed generally somewhat lower gelation ability as evident from Fig. S20 and Table S1 in ESI. ΔH values derived from Schröder–van Laar analysis for the melting process of **1** and *rac*- **1** hydrogel are 86.9 ± 3 and 94.4 ± 3 $kJ.mol^{-1}$, respectively (Fig. S21 in ESI). Positive values indicate that melting process is endothermic and leads to a system with higher entropy.

Furthermore, data show that the chiral segment influences the self-assembly process, which is more favorable for chiral sample **1**. Attempts for gel formation from derivatives **2** and **3** at concentration 1 wt% were unsuccessful for all attempted solvents. Moreover, both control derivatives (**2**, **3**) were sparingly soluble in water and well soluble in numerous organic solvents. Inspection of 0.5 wt % **1** xerogels made from water, toluene and isopropanol by scanning electron microscopy (SEM) and transmission electron microscopy (TEM) revealed the corresponding 1D nanofiber structures (Fig. 2), which differ in shape and size based on the solvent used. In water, we observed helical fiber sheets (Fig. 2; A, D) with thickness of 20 nm and width of 10 nm, while **1** in toluene formed fibrils with diameters of 50–80 nm entangled into large bundles (Fig. 2; B, E). Images of xerogels from isopropanol showed fibrous structures with diameter of ca. 20 nm (Fig. 2; C, F). UV–vis spectra of 0.2 wt% hydrogel of **1** in hot deionized water showed that the intensity of the absorption peak at 275 nm slightly decreases upon sample cooling, but a new peak at about 330 nm appears at the same time (Fig. 3A). Similar dramatic changes were observed in circular dichroism (CD) spectra (Fig. 3B). Namely, a peak at 220 nm with a positive value and signal maxima at 235 and 275 nm with negative values changed to peaks at 224, 260 and 336 nm with positive values and a signal at 313 nm with negative value upon sample cooling. This effect was even more pronounced in isopropanol (Fig. 3A inset, Fig. S24 and S25 ESI) and was present already at higher temperatures in toluene (Fig. S26 and S27 in ESI), indicating that the polar part of **1** is responsible for the spectroscopic change due to its mitigation upon interaction with protic solvent molecules. On the contrary, **2** and **3** showed no changes in UV–vis or CD spectra upon temperature sweep (Fig. S30 and S31 in ESI).

Additionally, we performed detailed ^1H, ^{13}C NMR analysis (Figs. S1-S8 in ESI) and temperature dependent (VT) ^1H NMR experiments (Fig. 3C). ^1H NMR peaks from the aromatic nicotinamide-based segment of **1** were seen in 10% H_2O/D_2O solution at 90 °C as a singlet at 9.60 (H-2), two doublets at 9.52 (H-6) and 9.27 (H-4) and a doublet of the doublet at 8.66 (H-5) ppm, in agreement with C_2 symmetric structure of monomeric **1** with cation–anion separation (similar ^1H NMR shifts were also observed in $CDCl_3$; see Figs. S1 and S6 in ESI). Upon cooling, intensities of the aromatic signals were lowered, and the peak for H-2 practically disappeared. Simultaneously, ^1H NMR resonances were shifted upfield and became very broadened with decreasing temperature. The most pronounced change appeared between 40 and 30 °C, in accordance with the gelation process (Fig. 3C). The absence of H-2 resonance in D_2O indicates the acidic nature of this hydrogen atom and its possible involvement in the self-assembly process. Similar behavior is observed for amidic hydrogen, which can be seen in the H_2O/D_2O solution as a broad singlet at 9.14 ppm (Fig. S6 in ESI). Contribution of different H bonding motives was supported by FTIR spectra of xerogels, where two distinct C=O stretching vibrations were observed at 1624 and 1645 cm^{-1} for hydrogel of **1** in water (Fig. 3D). This indicated a strong hydrogen bonding that corresponds to band at 1624 cm^{-1} and band at 1645 $cm^{-1}$with no or weak hydrogen bonding. The band at 1624 cm^{-1} remained at the same position in all samples that indicate a similar and stable strong hydrogen bonding in self-assembly (Fig. 3D). The later one was shifted to higher wavenumber for isopropanol and toluene to 1646 and 1647 cm^{-1}, respectively, indicating weaker degree of hydrogen bonding by decreasing the solvent polarity and thus it is expected that this carbonyl is exposed more to environment. On the other hand, the FTIR spectrum of **3** showed only one absorption peak for C=O at 1633 cm^{-1} (Fig. S23 in ESI).

Since attempts to obtain suitable single crystals for X-ray diffraction analysis were not successful, we performed DFT computational studies of **1** and its assemblies to understand key interactions in the gelation process at the molecular level. Akin to non-ionic bisamide gelators derived from cyclohexane-1,2-dicarboxylic acid or cyclohexane-1,2-diamines, self-assemblies of **1** prefer *anti* arrangement of two vicinal amidic groups over *syn* disposition (Fig. S33 in ESI). Surprisingly, apart from structures with amide–amide (CO···HN) hydrogen bonding across two polar strands of the self-assembly (Fig. 4, A), we found another lower-lying minima (Fig. 4, B and Figs. S33-S35 in ESI). Here, the self-assembly is held by amide–amide H-bonds, $d(CO\cdots HN)_{avrgd}$ = 1.82 Å, across one strand of the polar domain, while CO···HN interactions are superseded by bromide-mediated hydrogen bonds between amide and nicotine-based moieties across the second parallel strand, with averaged short C_2-H···Br (2.56 Å) and CONH···Br (2.42 Å) contacts. In addition to these interactions and van der Waals attraction between long alkyl chains, this structure is further supported by an electrostatic interaction between carbonyl oxygens and the strongly polarized H-4 atoms from nicotinamide-based segment, as evident from their distance (2.19 Å) and non-covalent interaction (NCI) [53–54] plot (Fig. 4 and Figs. S33 and S39 in ESI). The formation of a hybrid NH···OC and H···Br^- bonding pattern is facilitated by the electron deficient amidic and H-2 hydrogen atoms from nicotinamide-based segments (see NMR section above), which interact with excessive electron densities on both oxygen atoms and bromide anions, as also confirmed by NCI plots in Fig. 4, D and E. These donor–acceptor interactions

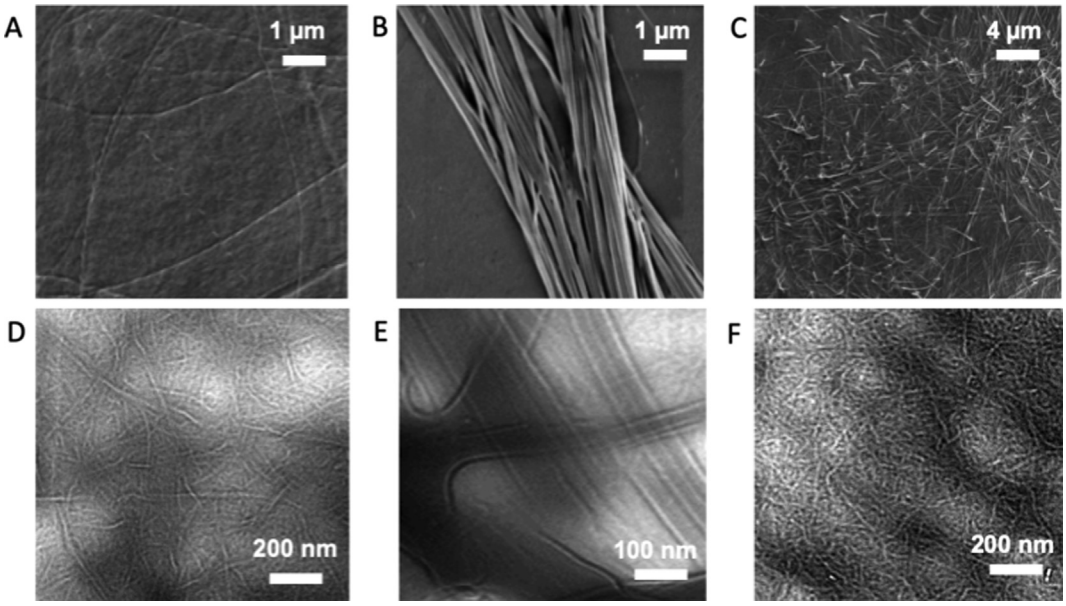

Fig. 2. SEM (A,B,C) and TEM (D,E,F) images for xerogels of **1** in water (A,D), toluene (B,E) and isopropanol (C,F). Concentration of gelation agent **1** is 0.5 wt% for all tests.

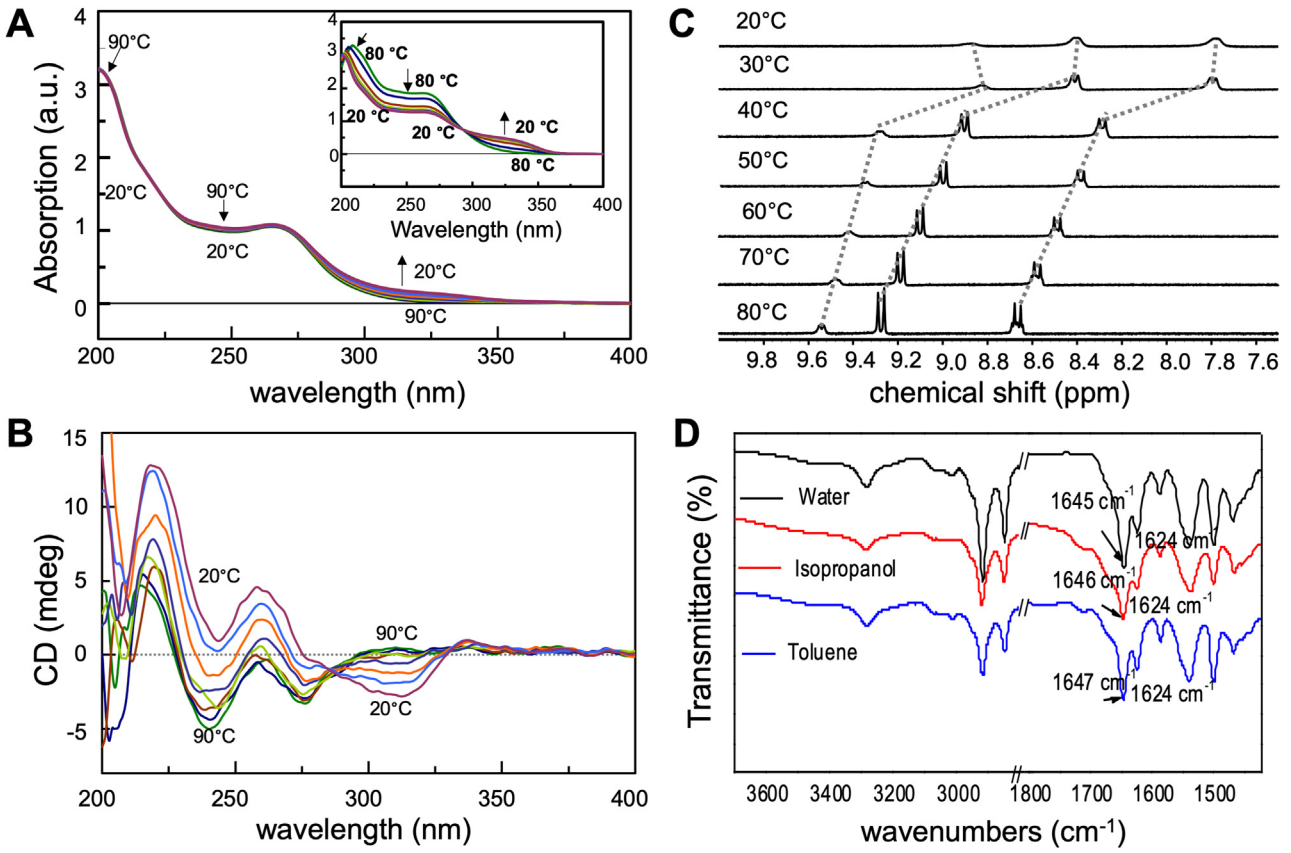

Fig. 3. A) UV–vis and B) circular dichroism (CD) spectra of gelation process for 0.2 wt% **1** in water; inset UV–vis spectra for 0.2 wt% **1** in propanol; C) VT ^{1}H NMR experiment of **1** in D_2O; D) FTIR for xerogel form **1** in water, toluene and isopropanol.

are also seen in the natural bond orbital (NBO) analysis as couplings between the occupied "lone-pair" (LP) orbitals on oxygen or bromide and antibonding $\sigma^*(N-H)$ and $\sigma^*(C_{2,pyridine}-H)$ orbitals, respectively. According to NBO second-order perturbation energy analysis for the structure given in Fig. 4, B, the averaged interaction energies for LP(O) → $\sigma^*(N-H)$, LP(Br) → $\sigma^*(N-H)$ and LP(Br) → $\sigma^*(C_{2,pyridine}-H)$ are 16.3, 11.5 and 6.3 kcal.mol^{-1}, respectively, hinting at the somewhat larger stabilization of mutual hydrogen bonds between bromide anion and "acidic" NH and CH groups than of single amide-amide interaction. In the case of trimers, tetramers and hexamers, the motif with a hybrid NH···OC and H···Br$^-$ bonding pattern is stabilized over the corresponding aggregates with

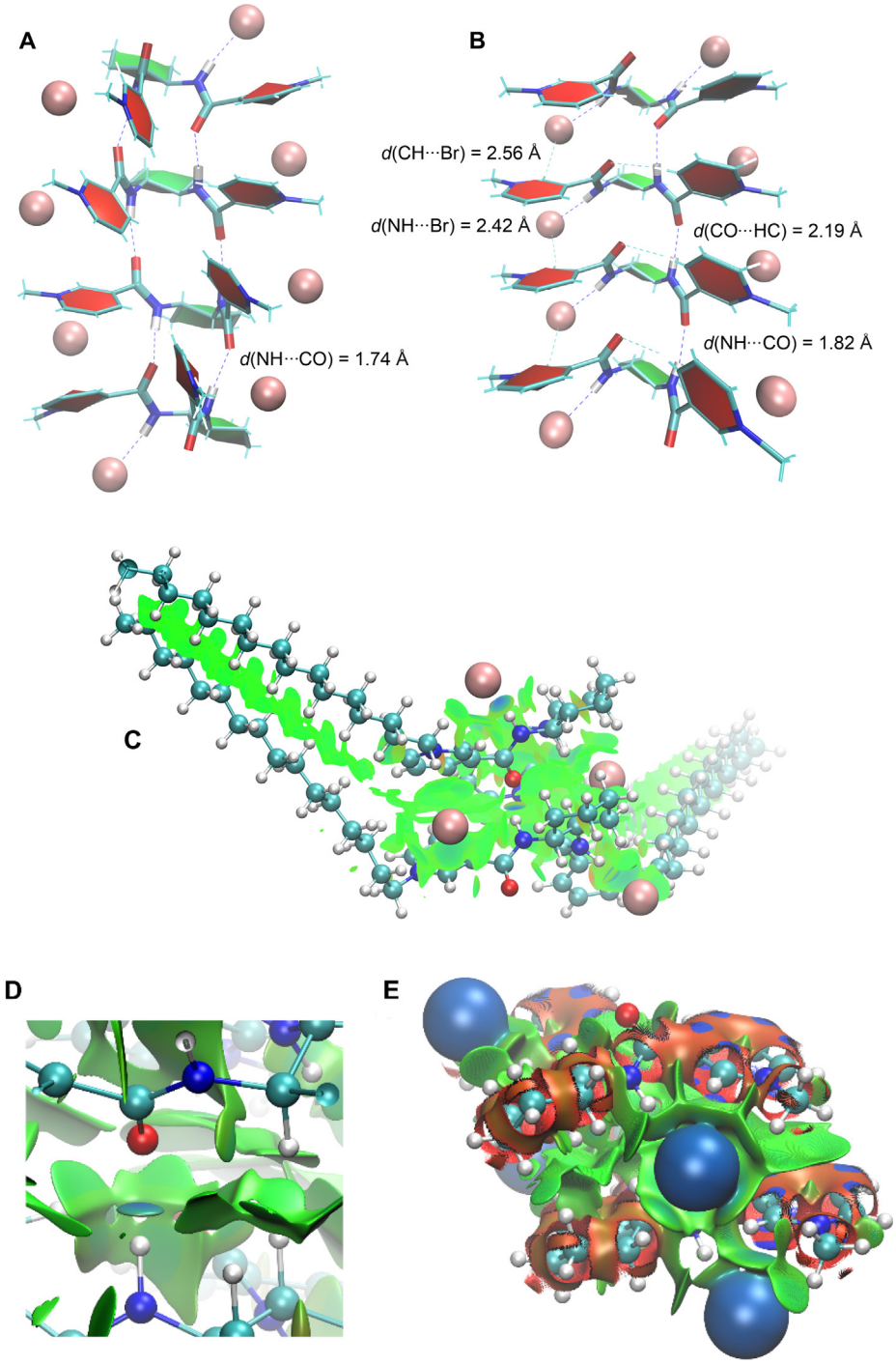

Fig. 4. DFT optimized structures of the tetrameric aggregates of **1** with only amide–amide H-bonds across the polar domain (A) and with a hybrid/asymmetric hydrogen bonding NH···OC and H···Br^- pattern (B). Truncated model with CH_3 groups instead of *n*-hexadecyl used for clarity. C) Three-dimensional NCI reduced density gradient (RDG) plot (isosurface value ± 0.3 au) of the non-covalent interaction regions in dimeric **1** with asymmetric hydrogen bonding. Regions with attractive forces in green and blue; D) Inset view at RDG plot (isosurface ± 0.4 au) with an apparent NH···CO interaction; E) View at RDG plot (isosurface ± 0.8 au) showing Br^-···HN and Br^-···HC interactions. See also Fig. S39 in ESI for selected individual NCI interactions. (For interpretation of the references to color in this figure legend, the reader is referred to the web version of this article.)

two parallel amide–amide strands by 11.4, 36.7 and 65.0 kJ.mol^{-1}, respectively. Note that the energetically preferred architecture (Fig. 4B) is supposed to display-two inequivalent CO groups, in accordance with two distinct carbonyl stretch vibrations observed experimentally (calculated bands are at 1630 and 1653 cm^{-1} for NH– and CH-interacting CO groups, respectively), and it also provides a better match between observed and DFT simulated CD spectra (Fig. 3B *vs* Figs. S41 and S42 in ESI). Close ion-pair contact between Br^- and amide moieties from nicotinamide-based segment in self-assemblies is also reflected in the appearance of the charge-transfer band at 330 nm, as assigned in computed TD-DFT spectra and upfield ^{1}H NMR shifts of the nicotine-based segment upon gelation (see Figs. S42- S44 in ESI). In keeping with expectations, the asymmetric NH···OC and C—H···X^- bonding pattern was not observed in our simulations when Br^- in **1** was replaced by a bulky and weakly-coordinating PF_6^- anion. At the same time,

CO···HN interactions were elongated (to 1.84 Å) when compared to the analogous structure in Fig. 4, A due to repulsion between insufficiently shielded, positively-charged nicotine-based moieties. This along with steric demands of the PF_6^- anion leads to the tilting of nicotine-based rings from their mutual parallel alignment (Fig. S36 in ESI) and thus hampers efficient interaction between long alkyl chains in the self-assembly. Replacement of the nicotinamide segments by regioisomeric isonicotinamide ones, while keeping bromide as a counterion, destabilized the structure with a hybrid (asymmetric) NH···OC and H···Br bonding pattern and led to the energetic preference of structure with only amide–amide H-bonds across the polar domain (Fig. S37 in ESI). These findings along with the fact that **2** and **3** possess no supergelation properties suggest that mutual presence of a nicotinamide-based segment and bromide ion is crucial in the mechanism of self-assembly and gel formation of these ionic compounds.

Encouraged by the supergelation ability of **1**, we investigated viscoelastic properties of corresponding gels. First, the strain sweep was scrutinized for 0.5 wt% **1** gels at constant frequency sweep (1 Hz) and temperature (25 °C). The experiments showed the condition where storage (G') and loss modulus (G") are independent from the applied strain and determine linear viscoelastic region. In water, this gel shows reversible network properties up to 0.5% strain (Fig. 5A). The crossover point is the indication of the strain tolerance for materials and shows fluid-like behavior at high strain amplitudes. The value for this irreversible network deformation is at 90% of applied strain, showing that **1** tolerates high mechanical force. Comparison of rheology of **1** and *rac*-**1** derivatives showed similar profiles for strain sweep, but stiffness was dramatically reduced by almost an order of magnitude in the former. This indicates that the chiral unit reduces stiffness, even though overall viscoelastic characteristics of gels are similar, in accordance with the gelation ability study (Fig. 5A). Isopropanol and toluene **1** gels are stiffer than **1** hydrogel, as indicated in reaching storage modulus at 0.1% strain at 100 and 200 kPa, respectively (Fig. 5B). Additionally, we performed thixotropic testing of **1** hydrogel (Fig. 5 C). Behavior of storage modulus (G') and loss modulus (G") was monitored for 0.5 wt% **1** hydrogel at constant frequency (1 Hz) and constant temperature (25 °C) using low strain (0.5%) altered by high strain (100%) for a duration of 50 s. Relatively slow recovery was observed, which indicates that observed changes require rearrangement in the hydrogel structure. Besides the thixotropic rheological test, hydrogel showed macroscopic recovery. After agitation with a bar gel, the solution became liquid-like, while after standing for a period of 5 h, stable hydrogel was recovered (Fig. 5 D upper). Moreover, samples of **1** are colorable, moldable and shape-persistent as indicated in Fig. 5D lower. After cutting to two types of cylinders —undoped (white) and doped (emerald green)— and pressing combined cylinders, the object fused to a large cylinder enabled a self-standing bridge formation, where light green color in the white part also indicates a diffusion of dye during a self-healing network process of hydrogel. Isopropanol gel showed similar behavior after fusion by pressing of undoped and doped (crystal violet) cylinders for an hour. Higher volatility of isopropanol showed continual evaporation of solvent that led to dry of gel within 240 mins (Fig. S32 ESI).

Since alcohols possess high octane number, environmental as well as economic advantages over petrol and diesel, they are frequently used as fuels for internal combustion engines or heat production. In this regard, we exploited isopropanol gel of **1** as a

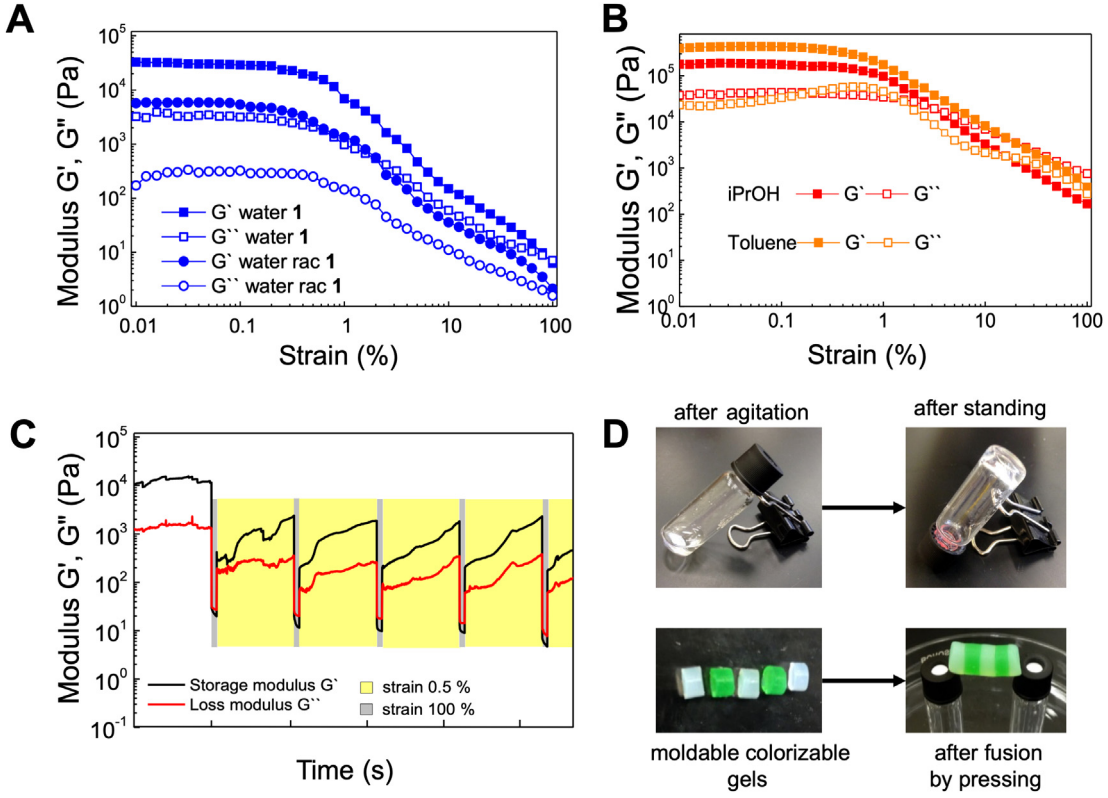

Fig. 5. Strain sweep A) for 0.5 wt% **1** and *rac*-**1** hydrogel and B) for isopropanol and toluene 0.5 wt% **1** gel; C) thixotropy-loop test for 0.5 wt% **1** hydrogels with alternating strain amplitudes of 100% (50 s, grey region) and 0.5% (300 s, yellow region) with constant frequency of 1 Hz; D) images showing moldable, colorable (emerald green) and shape-persistent hydrogel segments cut from a larger cylinder (left side) and a bridge over vials (right side) fabricated from five hydrogel cylinder blocks put together with and without dopped dye (emerald green). All tests were performed at 25 °C. (For interpretation of the references to color in this figure legend, the reader is referred to the web version of this article.)

quasi-solid fuel (Fig. 6A and Video S1 in ESI). Isopropanol was chosen due to its high gelation performance, low toxicity, low cost (ca. 0.8 $/kg), easy accessibility on the market and high combustion heat (2020 kJ.mol^{-1}). Moreover, transformation of liquid to gel suppresses issues with volatility, liquidity and spillage. Interestingly and importantly, the burning process of 0.5 wt% **1** isopropanol gel does not influence additional gelation process (Fig. 6B), and the molecular structure of **1** remains intact even after five consecutive burning cycles, with no signs of hydrolysis of amidic moiety or other chemical degradation (Fig. 6C). Fully repeatable gelation, low toxicity of isopropanol together with high flame resistance of **1**, attributable to bromide activity fire resistance during finalization of the burning process [55] and is advantageous over methanol-based fuel gels [12–13]. Previous reports show continous degradation from hydrolysis of ester group that limited application of such fuel gels in recyclability and up to our knowledge this is the first report on fully repeatable gemini gelator-based fuel gel. Furthermore, isopropanol gels of **1** are mechanically strong, self-healable, shape-modulated and colorable, which makes this application even more attractive. This gel is also non-explosive and not carcinogenic, so it can be applied as a fuel for interior as well as exterior heating.

4. Conclusions

In summary, an easily accessible nicotinamide-based gemini amphiphilic derivative **1** containing chiral cyclohexane-1,2-diamine-based segment shows supergelation ability in water and numerous polar protic, aprotic and non-polar solvents. Critical gelation concentration in water is as low as 0.035 wt% that leads to visible rigidification of almost 150,000 water molecules, which is close to the highest value obtained among low-molecular-weight hydrogelators. Unique combinations of dynamic hydrogen bonds between H-2 hydrogens from nicotinamide-based segment, amide functional groups and bromide ions were identified as a key parameter in the supergelation process, supporting classical intermolecular amide–amide interactions appearing across one strand of the self-assembly. Such self-assembly distinguishes **1** from its congener with hexafluorophosphate counterion (**2**) and regioisomeric analogue (**3**), which possess no such architecture of the polar domain or supergelation properties. **1** clearly also outperforms structurally related LMWGs derived from chiral cyclohexane-1,2-diamine or cyclohexane-1,2-dicarboxylic acid (with cgc of 3–50 mg.ml^{-1}) in various non-polar and polar solvents [51–52]. Additionally, eco-friendly isopropanol gel of **1** showed excellent performance as a safe, non-explosive, not carcinogenic, non-toxic and reusable fuel with self-healable, shape-modulated and colorable properties, making this system attractive also for interior and exterior decorative purposes, retaining its strong memory (supergelation ability) even after numerous burning cycles. To the best our knowledge, this is the first report on stable, non-degraded, repeatable organogelator for fuel gels since previously showed degradation due to hydrolysis and/or usage of methanol [12–13]. In the case of gel production upscaling, we expect no biocontamination due to large amount of isopropanol that is used in medical antibacterials swabs. Moreover, economic perspective and large production of **1** can be optimized due to renewable bioresource of nicotinamide segment from niacin (nicotinic acid) as vitamin B3. The modular structure of **1** allows further study on the influence of chirality unit to form novel supramolecular architecture. Additionally, tunability of structure proposed modification of length

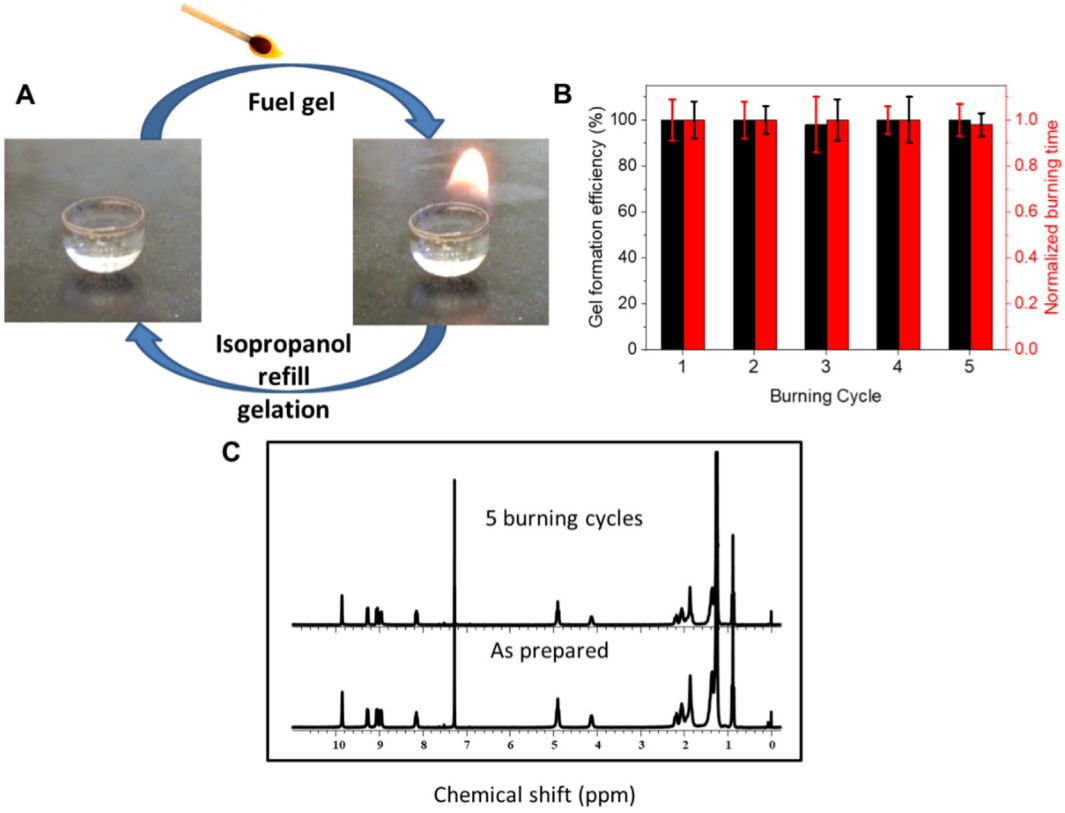

Fig. 6. A) Schematic representation of isopropanol gel of **1** as a quasi-solid and reusable non-toxic fuel; B) normalized burning time and gel formation efficiency in five repeated consecutive cycles; C) ^{1}H NMR of **1** after preparation and after five burning cycles. All tests were performed with 0.5 wt% isopropanol gel of **1**.

of alkyl aliphatic tail link to nicotine-based segment and exchange bromide to counterion with biologically active anions to control antibacterial and drug release properties, which are currently underway in our laboratories.

CRediT authorship contribution statement

Peter Kasak: Conceptualization, Formal analysis, Methodology, Writing - original draft, Writing - review & editing. **Peter Hrobárik:** Validation, Methodology, Resources, Writing - original draft, Writing - review & editing. **Josef Osička:** Data curation, Investigation, Writing - review & editing. **Dominika Soláriková:** Formal analysis, Investigation, Writing - review & editing. **Branislav Horváth:** Resources, Formal analysis, Investigation, Writing - review & editing. **Jan Tkac:** Resources, Writing - review & editing. **Kishor K. Sadasivuni:** Formal analysis, Investigation, Writing - review & editing. **Mariam A. AlMaadeed:** Resources, Writing - review & editing. **Roman Mikláš:** Conceptualization, Data curation, Writing - original draft, Writing - review & editing.

Declaration of Competing Interest

The authors declare that they have no known competing financial interests or personal relationships that could have appeared to influence the work reported in this paper.

Acknowledgements

This publication was jointly supported by Qatar University and Chemical Institute, Slovak Academy of Sciences Grant IRCC-2020-004. The findings achieved herein are solely the work of the authors. This work was supported by the Slovak Research and Development Agency (grant no. APVV-17-0324) as well as by the Grant Agency of the Ministry of Education of the Slovak Republic (VEGA projects no. 1/0712/18 and 1/0145/20). P.H. also acknowledges the support from the European Union's Horizon 2020 research and innovation programme under grant no. 810701. J.O. acknowledges the Ministry of Education, Youth and Sports of the Czech Republic—DKRVO (RP/CPS/2020/003). Authors thank to Dr. Emil Švajdlenka, Faculty of Pharmacy, Comenius University in Bratislava for HRMS measurements and Center for Advanced Materials and Gas Processing Center at Qatar University for support with facilities. The publication of this article was funded by the Qatar National Library.

Appendix A. Supplementary material

Supplementary data to this article can be found online at https://doi.org/10.1016/j.jcis.2021.06.071.

References

[1] F. Rodriguez-Llansola, B. Escuder, J.F. Miravet, J. Am. Chem. Soc. 131 (2009) 11478–11484.
[2] X. Du, J. Zhou, J. Shi, B. Xu, Chem. Rev. 115 (2015) 13165–13307.
[3] M.J. Webber, E.A. Appel, E.W. Meijer, R. Langer, Nature Mat. 15 (2016) 13–26.
[4] I.O. Shklyarevskiy, P. Jonkheijm, P.C.M. Christianen, A.P.H.J. Schenning, A. Del Guerzo, J.-P. Desvergne, E.W. Meijer, J.C. Maan, Langmuir 21 (2005) 2108–2112.
[5] S.S. Babu, V.K. Praveen, A. Aiayaghosh, Chem. Rev. 114 (2014) 1973–2129.
[6] N.M. Sangeetha, U. Maitra, Chem. Soc. Rev. 34 (2005) 821–836.
[7] A. Forget, T. Derme, D. Mitterberger, M. Heiny, C. Sweeney, L. Mudili, T.R. Dargaville, V.P. Shastri, Emergent Mat. 2 (2019) 233–243.
[8] R.G. Weiss, J. Am. Chem. Soc. 136 (2014) 7519–7530.
[9] B.O. Okesola, D.K. Smith, Chem. Soc. Rev. 45 (2016) 4226–4251.
[10] J. Cao, Y.-C. Zhang, L. Pan, C. Shi, X. Zhang, J.-J. Zou, Propellants Explos. Pyrotech. 45 (2020) 1018–1025.
[11] G. Corey Garland, Alcohol Fuel Gels, Colgate Palmolive Co., 1966, patent no. US3271120A.
[12] S. Bera, D. Haldar, J. Mater. Chem. A 4 (2016) 6933–6939.
[13] K. Bhaskar Pal, B. Mukhopadhyay, ChemistrySelect 2 (2017) 967–974.
[14] M. Zheng, A. Jaramillo-Botero, X.-H. Ju, W.A. Goddard, III Phys, Chem. Chem. Phys 23 (2021) 10909–10918.
[15] M. Baglioni, J.A.L. Domingues, E. Carretti, E. Fratini, D. Chelazzi, R. Giorgi, P. Baglioni, A.C.S. Appl, Mater. Interfaces 10 (2018) 19162–19172.
[16] A.H. Clark, Structural and mechanical properties of biopolymer gels. in Food Polymers, Gels and Colloids Ed. E. Dickinson, Woodhead publishing (1991) 322–338.
[17] T.P. Santos, R.L. Cunha, Carbohydr. Polym. 192 (2018) 111–117.
[18] J. Alipal, N.A.S. Mohd Pu'ad, T.C. Lee, N.H.M. Nayan, N. Sahari, H. Basri, M.I. Idris, H.Z. Abdullah, Mater. Today: Proceedings 42 (2021) 240–250.
[19] P.R.A. Chivers, D.K. Smith, Nat. Rev. Mater. 4 (2019) 463–478.
[20] A. Panja, K. Ghosh, New J. Chem. 42 (2018) 13718–13725.
[21] H.C. Geiger, M. Lamson, D.J. Galka, Langmuir 30 (2014) 13979–13986.
[22] C. Yu, M. Xue, K. Liu, G. Wang, Y. Fang, Langmuir 30 (2014) 1257–1265.
[23] A. Aggeli, M. Bell, N. Boden, J.N. Keen, P.F. Knowles, T.C.B. McLeish, M. Pitkeathly, M. Radford, Nature 386 (1997) 259–262.
[24] A.D. Martin, P. Thordarson, J. Mater. Chem. B 8 (2020) 863–877.
[25] J.P. Wojciechowski, A.D. Martin, E.Y. Du, C.J. Garvey, R.E. Nordon, P. Thordarson, Nanoscale 12 (2020) 8262–8267.
[26] G.-F. Liu, W. Ji, W.-L. Wang, Ch.-L. Feng, A.C.S. Appl, Mater. Interfaces 7 (2015) 301–307.
[27] S. Ghosh, R.D. Mahapatra, J. Dey, Langmuir 30 (2014) 1677–1685.
[28] H. Hoshizawa, Y. Minemura, K. Yoshikawa, M. Suzuki, K. Hanabusa, Langmuir 29 (2013) 14666–14673.
[29] Ch. Yin, F. Jiang, L. Wu, B. Li, Soft Matter 15 (2019) 5034–5041.
[30] N. Cheng, Q. Kang, J. Xiao, N. Du, L. Yu, J. Colloid Interface Sci. 511 (2018) 215–221.
[31] V.A. Mallia, H.-I. Seo, R.G. Weiss, Langmuir 29 (2013) 6476–6484.
[32] F. ÓAnna, P. Vitale, S. Marullo, R. Noto, Langmuir 28 (2012) 10849–10859.
[33] N. Basu, A. Chakraborty, R. Ghosh, Gels 4 (2018) 52–86.
[34] I.S. Okafor, G. Wang, Carbohydrate Research 451 (2017) 81–94.
[35] N. Minakuchi, K. Hoe, D. Yamaki, S. Ten-no, K. Nakashima, M. Goto, M. Mizuhata, T. Maruyama, Langmuir 28 (2012) 9259–9266.
[36] R.J.H. Hafkamp, M.C. Feiters, R.J.M. Nolte, J. Org. Chem. 64 (1999) 412–426.
[37] F. Fages, F. Vögtle, M. Žinić, Top. Curr. Chem. 256 (2005) 77–131.
[38] Y. Jeong, K. Hanabusa, H. Masunaga, I. Akiba, K. Miyoshi, S. Sakurai, K. Sakurai, Langmuir 21 (2005) 586–594.
[39] N. Zweep, A. Hopkinson, A. Meetsma, W.R. Browne, B.L. Feringa, J.H. van Esch, Langmuir 25 (2009) 8802–8809.
[40] N. Mohmeyer, H.-W. Schmidt, Chem. Eur. J. 13 (2007) 4499–4509.
[41] M. Rajeswara Rao, S.-S. Sun, Langmuir 29 (2013) 15146–15158.
[42] B.L. Schottel, H.T. Chifotidesa, K.R. Dunbar, Chem. Soc. Rev. 37 (2008) 68–83.
[43] A. Frontera, P. Gamez, M. Mascal, T.J. Mooibroek, J. Reedijk, Angew. Chem. Int. Ed. 50 (2011) 9564–9583.
[44] H.T. Chifotides, K.R. Dunbar, Acc. Chem. Res. 46 (2013) 894–906.
[45] G.O. Lloyd, J.W. Steed, Nat. Chem. 1 (2009) 437–442.
[46] D. Ghosh, I. Lebedyte, D.S. Yufit, K.K. Damodaran, J.W. Steed, CrystEng Comm 17 (2015) 8130–8138.
[47] T. Knaus, C.E. Paul, C.W. Levy, S. de Vries, F.G. Mutti, F. Hollmann, N.S. Scrutton, J. Am. Chem. Soc. 138 (2016) 1033–1039.
[48] W. Xiao, R.-S. Wang, D.E. Handy, J. Loscalzo, Antioxid. Redox, Signal. 28 (2018) 251–272.
[49] K.M. Ralto, E.P. Rhee, S.M. Parikh, Nat. Rev. Nephrol. 16 (2020) 99–111.
[50] U. Gran, O. Wennerström, G. Westman, Tetrahedron Asymmetry 11 (2000) 3027–3040.
[51] K. Hanabusa, M. Yamada, M. Kimura, H. Shirai, Angew. Chem. Int. Ed. 35 (1996) 1949–1951.
[52] B. Pi-Boleda, M. Sans, M. Campos, P. Nolis, O. Illa, J.C. Estévez, V. Branchadell, R. M. Ortuño, Chem. Eur. J. 23 (2017) 3357–3365.
[53] E.R. Johnson, S. Keinan, P. Mori-Sánchez, J. Contreras-García, A.J. Cohen, W. Yang, J. Am. Chem. Soc. 132 (2010) 6498–6506.
[54] J. Contreras-García, E.R. Johnson, S. Keinan, R. Chaudret, J.-P. Piquemal, D.N. Beratan, W. Yang, J. Chem. Theory Comput. 7 (2011) 625–632.
[55] M. Alaee, R.J. Wenning, Chemosphere 46 (2002) 579–582.